Development and analysis of wafer-bonded four-junction solar cells based on antimonides with 42 % efficiency under concentration

Felix Predan[1], Oliver Höhn[1], David Lackner[1], Alexander Franke[1], Henning Helmers[1] and Frank Dimroth[1]

[1]Fraunhofer Institute for Solar Energy Systems ISE, Heidenhofstrasse 2, 79110 Freiburg, Germany

***Abstract* - The highest solar cell efficiencies today are reached with four-junction devices under concentrated illumination. The optimal bandgap combination for realistic four-junction cells is modelled to be 1.89/1.42/1.05/0.68 eV and indeed promises for efficiencies > 50 %. We present the development and analysis of a wafer-bonded four-junction solar cell based on GaInP/GaAs/GaInAs//GaInAsSb. This concept allows for the implementation of these ideal bandgaps and exhibits at present an efficiency of 42.0 ± 2.5 % at a concentration of 599x AM1.5d. The present loss mechanisms in this device are analyzed, which are dominated by current losses due to mismatched subcell currents and absorbing passive layers. Under the assumption of proper current matching, this device would achieve an efficiency above 44 %.**

***Index Terms* — multi-junction solar cells, four-junction solar cells, antimonides, wafer bonding, MOVPE.**

I. Introduction

Great efforts are taken to maximize the conversion efficiency of photovoltaic devices - a key parameter to minimize the levelized costs of electricity. Multi-junction solar cells based on III-V compound semiconductors currently exhibit the highest conversion efficiencies [1], and are applied in concentrating photovoltaics and in space. Materials with decreasing bandgaps are stacked on top of each other, successively absorbing the broadband solar spectrum. This significantly reduces the thermalization and transmission losses compared to single-junction solar cells. The state-of-the-art multi-junction cell product is a GaInP/GaInAs/Ge three-junction cell, reaching an efficiency up to 41.6 % under concentration [2, 3].

Even higher conversion efficiencies are achievable by increasing the number of p-n junctions in the device. The highest reported efficiency so far of 46.1 % under concentration of 312 suns was achieved by a wafer-bonded four-junction solar cell combining III–V materials on GaAs and InP [4]. A comparably high efficiency of 45.6 % at 690 suns was obtained with an inverted metamorphic four-junction cell structure based on GaAs [5].

Here, we present on the development and analysis of a wafer-bonded cell based on GaInP/GaAs/GaInAs//GaInAsSb ("//" refers to the position of the wafer-bond), which is sketched in Fig. 1. With the quaternary material $Ga_{0.98}In_{0.02}As_{0.018}Sb_{0.982}$ an optimal bandgap of 0.68 eV for 2-terminal four-junction devices under concentration can be realized. Accordingly, the concept has the potential for achieving efficiencies > 50 %, as discussed in section II. The potential is higher than for Ge-based multi-junction cells due to the direct bandgap of GaInAsSb which enables a higher absorption, therefore thinner layers and consequently lower voltage losses.

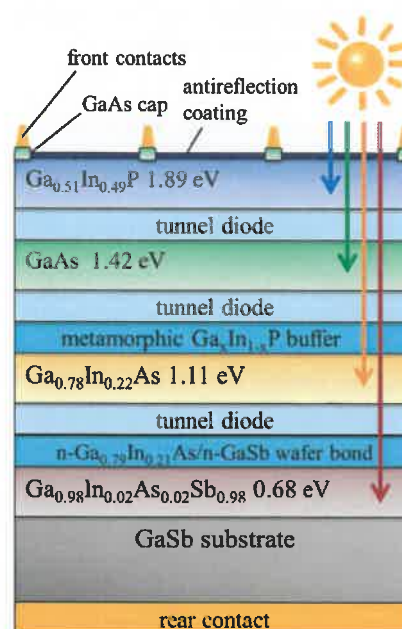

Fig. 1. Sketch of a wafer-bonded, 2-terminal $Ga_{0.51}In_{0.49}P$/GaAs/$Ga_{0.78}In_{0.22}As$//$Ga_{0.98}In_{0.02}As_{0.02}Sb_{0.98}$ four-junction solar cell.

Lumb *et al.* demonstrated the high potential of Sb-based multi-junction cells in their work on a mechanically stacked, 4-terminal GaInP/GaAs/GaInNAsSb/GaSb/GaInAsSb cell grown by molecular beam epitaxy. Under concentrated sunlight, the top three junctions achieved an efficiency of 42.8 % and the two bottom cells additionally contribute 1.7 %, resulting in an overall efficiency of 44.5 % [6].

In our approach, the direct wafer bonding results in a monolithically integrated 2-terminal device. This comes with the challenge of matching the currents of each of the subcells. Otherwise, the integration of 2-terminal devices into modules is easier and more cost-effective, compared to cells with four terminals. All materials in this work are grown in industrial-sized MOVPE reactors, meaning the cell is applicable to an industrial manufacturing environment and therefore suitable for all applications of advanced III-V multi-junction solar cells

including concentrating photovoltaics. Some developments for the Sb-based four-junction cell have been described already in Ref. [7]. The descriptions include the wafer-bonding, the metallization of p-GaSb and the growth of highly efficient GaSb-based bottom cells with $Al_{0.2}Ga_{0.8}As_{0.02}Sb_{0.98}$ barriers.

The presented paper is significantly extended and begins with a modelling study in section II, which is divided into two parts. First, optimal bandgap combinations are modelled for realistic multi-junction solar cells with two terminals. In the second part, an even more accurate efficiency target is determined for the Sb-based four-junction cell, taking into account losses that have already been achieved for single cell components. In the experimental section III, the processing of the device is described, addressing the numerous challenges in fabricating highly efficient Sb-based four-junction solar cells. The results of the processed devices are presented and discussed in chapter IV. The main loss mechanisms are quantified and an outlook for further improvements of the concept is given.

II. Theoretical Modelling

The optimal bandgap combinations and efficiency potentials for monolithic solar cells with four-, five- and six-junctions are derived for a 500x concentration (AM1.5d [8], 1000W/m²) at 25° C. Detailed balance calculations [9] have been already applied in that context [9, 10] and this "radiative limit" also represents the first examined case in this study. The approach assumes a binary external quantum efficiency (*EQE*) of 1 for photons with an energy above the bandgap and 0 below. Further, solely voltage losses from radiative recombination are taken into account, assuming 100% external radiative efficiency. Other losses that occur in real solar cells such as parasitic resistances, non-radiative recombination and optical losses (shading, reflection, finite spectral absorbance) are neglected [11].

The findings are depicted in Fig. 2, in which the efficiency potential of cells with four to six series connected junctions is plotted as a function of the bottom cell bandgap. The calculated optimal bandgap combinations for the radiative limit are in agreement to former results [10] - small differences are attributed to differences in the applied numerical model (spectral discretization etc.). An important observation of Fig. 2 is that the atmospheric absorption band in the AM1.5d spectrum between ~0.64 and ~0.69 eV results in two local efficiency maxima. One lies in the range of a bottom cell bandgap between ~0.51 and ~0.56 eV and one is close to ~0.69 eV. We want to emphasize that both of these maxima show a very similar efficiency potential. As a consequence, small changes in the assumed voltage loss can have a great impact on the resulting optimum bandgap for the bottom cell.

To exemplify this statement, a second "empiric potential" case is considered in Fig. 2. This case is based on the same assumptions as the "radiative limit", with the exception of a 90 mV voltage loss to the radiative limit for each junction. As discussed below, that value represents the lowest voltage loss that has been reported in literature for solar cells without rear side mirror (based on GaInP [12] and GaAs [13, 14]) in the relevant range of current density.

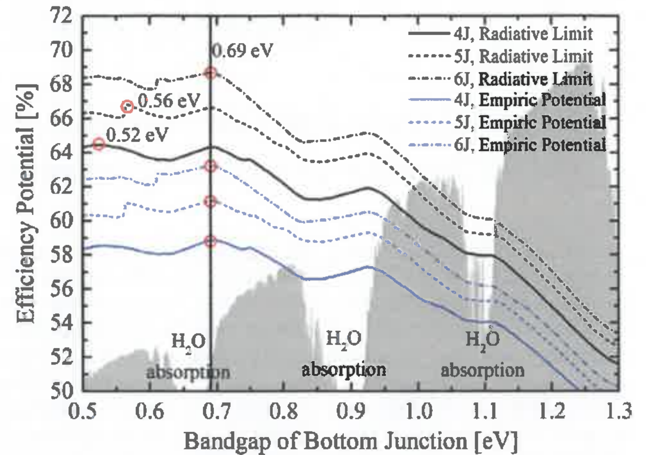

Fig. 2. Efficiency potentials for 4-, 5- and 6-junction (J) solar cells at a concentration of 500x AM1.5d, plotted as a function of the bottom cell bandgap. The values are calculated for the "radiative limit" and a "empiric potential". The optimal bottom cell bandgap is highlighted with a red circle and the AM1.5d spectrum is depicted in grey.

In the "radiative limit", the optimal bottom cell bandgap for 4-, 5-, and 6-junction solar cells is 0.52, 0.56 and 0.69 eV, respectively. However, in the "empiric potential" case the optimal bottom cell bandgap sticks to 0.69 eV, as the higher voltage loss favors junctions with higher bandgaps (similar voltage losses lead to lower relative efficiency losses for higher bandgaps). The quantitative outcome of this effect is further illustrated in Fig. 3.

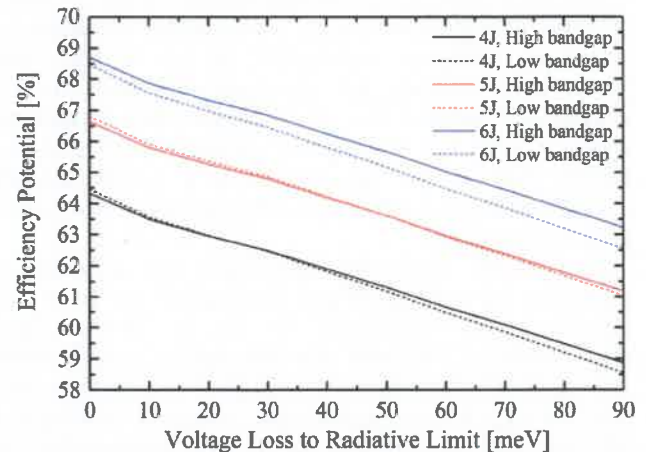

Fig. 3. Efficiency potentials for 4-, 5- and 6-junction (J) solar cells at 500x AM1.5d, plotted as a function of the assumed voltage loss to the radiative limit for each junction. "Low bandgap" stands for the efficiency maximum at a bottom cell bandgap between ~0.51 and ~0.56 eV and "high bandgap" for the maximum at 0.69 eV.

Fig. 3 directly compares the efficiency potential for bottom cell bandgaps between ~0.51 and ~0.56 eV ("low bandgap")

to the efficiency potential at 0.69 eV ("high bandgap") for varying losses to the radiative limit. As can be seen, the low bottom cell bandgap only becomes favorable for 4-, and 5-junction devices if the voltage loss to the radiative limit is reduced to below 30 and 55 mV, respectively. The realization of such low voltage losses would require (in addition to negligible defect recombination) the implementation of omnidirectional reflectors below each subcell [12, 13], which does not seem feasible based on today's technologies.

The ideal bandgap combinations and efficiency potentials for the "empiric potential" case are summarized in Table I. The result is an important update to the state-of-the-art, since it defines a 0.69 eV bottom subcell as the target for realistic multi-junction solar cells with 2-terminals. In other words, no improvement can be expected from implementing a bottom cell bandgap between 0.51 and 0.56 eV, compared to a 0.69 eV bottom cell. Further real-world losses in fill factor or current would not significantly alter the optimal bandgap combination. This holds also for varying operating temperatures – in this case the ideal set of bandgaps has to be reached under operating conditions.

A GaInP/GaAs/GaInAs//GaInAsSb cell enables the optimal combination of bandgap energies for a four-junction cell, and by that, promises for highest efficiencies. However, further losses, e.g. due to non-radiative recombination, parasitic resistances, shading and reflection are encountered in real devices. Therefore, a real-world efficiency target has been estimated for the Sb-based cell concept, assuming the lowest losses that have already been achieved elsewhere in III-V solar cell devices. It should be noted that this efficiency target is by definition arbitrary. Still, it is based on already demonstrated data and so yields a lower bound for what can be expected to be achievable with further R&D efforts and optimization.

The assumed parasitic resistances are a total serial resistance of 15 mΩcm^2 and a parallel resistance of 100 kΩ. The subcell current of 14.03 mA/cm^2 is calculated from the simulated absorption using real material absorption data and a code based on the transfer matrix method, which is discussed in Ref. [4]. The calculation takes into account 3 % shading by the front contacts and an anti-reflection coating (ARC) consisting of 121 nm MgF_2 and 79 nm Ta_2O_3 on a 30 nm AlInP window (compare Fig. 5).

When selecting reasonable subcell voltages for the modelling, different effects have to be considered. Assuming a simple 1-diode model, the open-circuit voltage V_{OC} of an ideal solar cell under concentration C increases according to:

$$V_{OC}(C) = \frac{n_{id}k_BT}{q} ln\left(\frac{CI_{ph}}{I_0}\right) = \frac{n_{id}k_BT}{q} ln\left(\frac{I_{ph}}{I_0}\right) + \frac{n_{id}k_BT}{q} ln(C) \quad (1)$$

n_{id} represents the ideality factor, k_B the Boltzmann constant, T the temperature, q the elemental charge, I_{ph} the photo-induced current and I_0 the dark current. The last summand in Eq. (1) is device-independent (for n_{id} = 1) and results in a ~160 mV voltage increase (per junction) for a 500x concentration at 25 °C. This effect is also considered in the calculation of the radiative limit, i.e. the loss to the radiative limit is in a first approximation C-independent. For real materials, further influences have to be considered - e.g. non-radiative defects saturate under concentration (see section IV). Therefore, the assumed voltage losses to the radiative limit are based on the lowest state-of-the-art values under concentration without backside mirror. The current density of a four-junction solar cell at 500x AM1.5d typically amounts to ~5 A/cm^2. In this current density range, the lowest reported voltage losses to the radiative limit are ~90 mV for GaInP [14], ~90 mV for GaAs [15, 16], ~100 mV for GaInAs [17] and ~120 mV for GaInAsSb [18, 19]. The resulting real-world efficiency target is listed in Table I and is 50.8% for the Sb-based 4-junction solar cell.

Table I. Optimal bandgap combination and efficiency for 4-, 5- and 6-junction solar cells for the "empiric potential" case and real-world efficiency target for the Sb-based four-junction cell. The values are calculated for a concentration of 500x (AM1.5d spectrum, 1000 W/m²) at 25 °C.

Device Concept & bandgap combination [eV]	J_{SC} [mA/cm^2]	V_{OC} [V]	FF [%]	η [%]
4-Junction, Empiric Potential 1.92/1.43/1.03/0.69	15.54	4.27	88.8	58.9
5-Junction, Empiric Potential 2.06/1.60/1.25/0.98/0.69	12.43	5.53	89.2	61.2
6-Junction, Empiric Potential 2.17/1.73/1.43/1.17/0.94/0.69	10.34	6.84	89.4	63.2
Sb-based 4-Junction Real-world Efficiency Target 1.89/1.42/1.05/0.68	14.03	4.21	86.1	50.8

As can be seen in Table I, small deviations (<0.03 eV) occur between the optimal bandgaps for the "empiric potential" and the "real-world efficiency target". The reason for this behaviour is that binary QEs with abrupt absorption edges and no reflection are assumed for the cell in the "empirical potential" whereas the real-world efficiency target accounts for non-abrupt absorption edges as well as a real ARC, exhibiting parasitic reflection (as shown in Fig. 5).

III. EXPERIMENTAL

The direct growth of a $Ga_{0.51}In_{0.49}P/GaAs/Ga_{0.78}In_{0.22}As//Ga_{0.98}In_{0.02}As_{0.02}Sb_{0.98}$ four-junction cell would result in high dislocation densities due to the high lattice mismatch of 6.4 % between $Ga_{0.78}In_{0.22}As$ and GaSb. Consequently, two separate epitaxial growths were performed and the subcells combined by direct wafer bonding. The fabrication scheme of the cell is illustrated in Fig. 4.

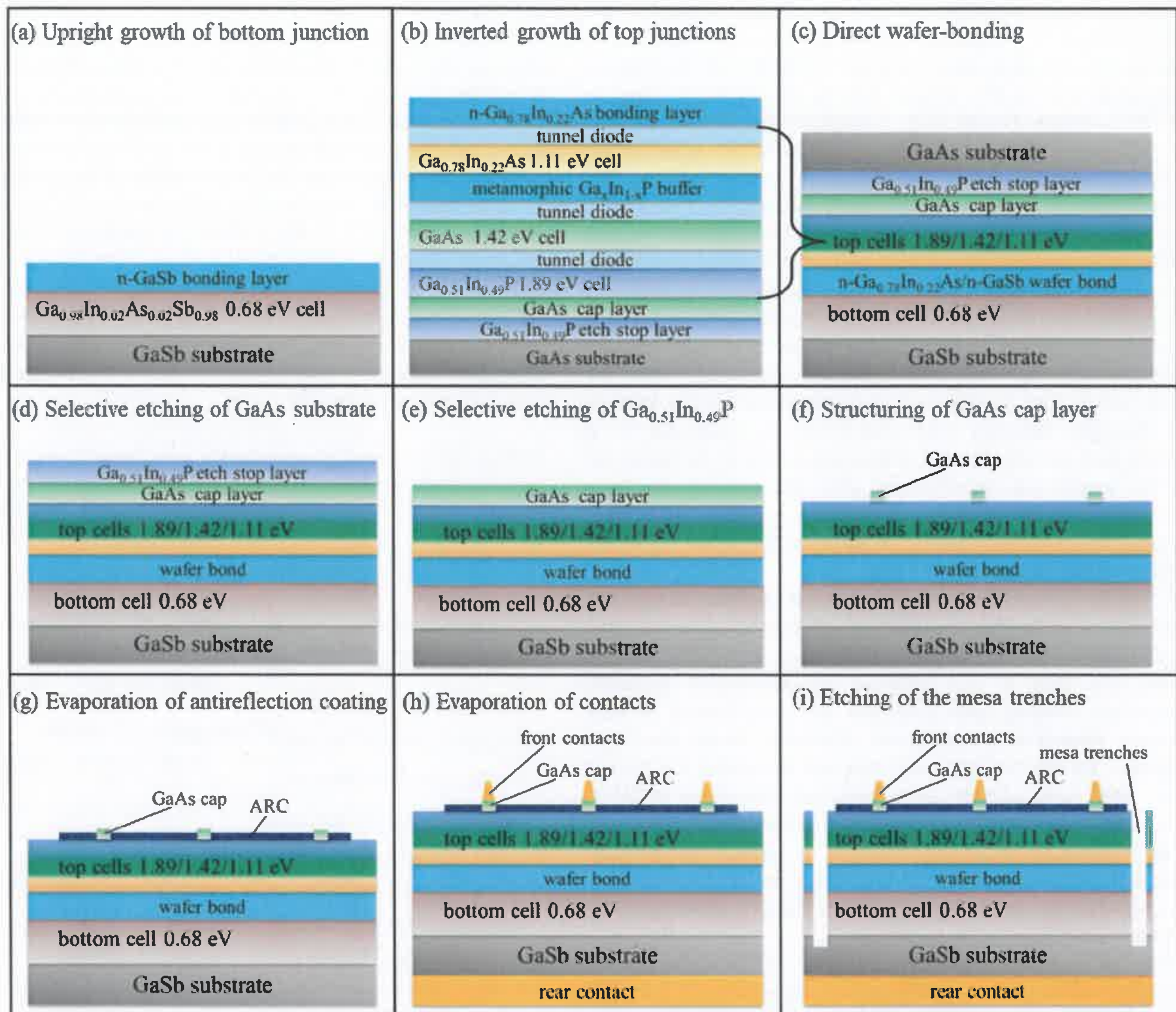

Fig. 4. Fabrication scheme for the wafer-bonded $Ga_{0.51}In_{0.49}P$/GaAs/ $Ga_{0.78}In_{0.22}As$//$Ga_{0.98}In_{0.02}As_{0.02}Sb_{0.98}$ four-junction solar cell.

Bottom junction growth, Fig. 4 (a): The Sb-based cell was grown upright on a p-GaSb substrate (oriented (100) 4° off toward (111)A) in a 7 x 4" CRIUS Close Coupled Showerhead reactor from Aixtron. The nominally 2500 nm thick $Ga_{0.98}In_{0.02}As_{0.018}Sb_{0.982}$ absorber has a 0.68 eV bandgap and is lattice-matched to GaSb. Barrier layers consisting of $Al_{0.20}Ga_{0.80}As_{0.02}Sb_{0.98}$ (1.0 eV bandgap, lattice-matched to GaSb) are used for carrier confinement. The topmost layer is the n-GaSb bonding layer, where parasitic light absorption can´t be avoided, as discussed below in the context of Fig. 5. Further details about the antimonide growth in a showerhead reactor have been published elsewhere [20, 21].

Top junctions growth, Fig. 4 (b): The $Ga_{0.51}In_{0.49}P$/GaAs/ $Ga_{0.78}In_{0.22}As$ 3-junction cell was grown inverted on an n-GaAs substrate (oriented (100) 6° off toward (111)B) in an Aixtron 2800-G4 TM reactor with a 8 x 4" configuration. The 1.89 eV $Ga_{0.51}In_{0.49}P$ cell with an intended thickness of 750 nm and the semi-transparent 1.42 eV GaAs cell (nominal thickness of 1770 nm) were grown lattice-matched on the GaAs substrate. Then, metamorphic $Ga_{1-x}In_xP$ buffer layers with increasing Indium content were deposited, which allow for a gradually change of the in-plane lattice constant between 5.65 Å and 5.73 Å for the subsequent GaInAs cell growth. The $Ga_{0.78}In_{0.22}As$ absorber was tuned to an intended bandgap of 1.11 eV and a nominal thickness of 2800 nm. Three tunnel-diodes connect all subcells in series and the topmost layer is an n-$Ga_{0.78}In_{0.22}As$ bonding layer.

Wafer Bonding, Fig. 4 (c): The subcells were combined by argon-beam activated wafer bonding. The method enables optical transparency, together with a high interfacial conductivity, which has been proven for a wide range of III-V semiconductors including antimonides [22–24]. The first step was the chemical-mechanical polishing (CMP), providing surfaces with solely few particles and low RMS roughness < 1 nm, which are mandatory for direct wafer bonding [25].

The wafers were sputtered in an Ayumi SAB-100 bonder in ultra-high vacuum (< 3 x 10^{-6} Pa) to remove oxides and contaminants. The process results in a thin amorphous surface layer with dangling bonds. Subsequently, the wafers were pressed together so that covalent bonds are formed, permanently joining the semiconductors. Optimized process parameters and annealing conditions enabled a resulting bond resistance of 3.3 ± 1.3 mΩcm^2 at the n-GaSb/n-$Ga_{0.78}In_{0.22}As$ interface [24]. This bond resistance does not significantly compromise the cell performance: even at 500x concentration, resulting in a current density of ~5 A/cm^2, the expected voltage loss at the bond interface is < 20 mV.

GaAs substrate & $Ga_{0.51}In_{0.49}P$ etching, Fig. 4 (d, e): The GaAs substrate was removed by selective wet-chemical etching in a solution of NH_3/H_2O_2. A $Ga_{0.51}In_{0.49}P$ etch stop layer was subsequently removed selectively in HCl.

GaAs cap structuring, Fig. 4 (f): A 400 nm n-GaAs cap layer enables low front contact resistances and prevents metal diffusion into the active solar cell region. A photoresist was structured to protect the parts of the wafer, where the front grid will be evaporated. Subsequently, the uncovered GaAs was selectively etched with a solution of $C_6H_8O_7/H_2O/H_2O_2$, revealing the AlInP window layer.

ARC deposition, Fig. 4 (g): An ARC consisting of 121 nm MgF_2 on top of 79 nm Ta_2O_3 was deposited in a Pfeiffer PLS 570 evaporator in order to provide low reflectance over a spectral range from 500 to 1900 nm.

Contact deposition, Fig. 4 (h): Metal contacts were evaporated in a Classic 590 evaporator from Pfeiffer. The p-GaSb substrate is fully metallized with a 2.1 µm thick Pd/Au/Ag metal stack, enabling reproducible rear contacts with specific resistances in the range of a few 10^{-5} Ωcm^2 [21]. The front contacts are based on a 2.1 µm thick metal stack of Pd/Au/Ge/Ti/Pd/Ag, resulting in contact resistances in the range of 10^{-6} Ωcm^2. The front contacts were structured by means of a lift-off process using a negative resist.

Mesa etching, Fig. 4 (i): The final step was the etching of the mesa trenches to electrically separate the concentrator cells (size of ~6 mm^2). A structured photoresist was used as the etching mask. The arsenides and phosphides in the top three junctions were etched using a solution of $HBr/H_2O_2/H_2O$. A second $H_2O/C_6H_8O_7/H_3PO_4/H_2O_2$ etchant was applied to etch few micrometres into the GaSb substrate.

Cell Characterization: The four-junction cells were measured at the Fraunhofer ISE CallLab. Quantum efficiency (*QE*) measurements are performed at a spectrally adjustable setup at 25 °C [26, 27]. The absolute height of the quantum efficiency was corrected with the 1-sun current density measured under a spectrally adjustable solar simulator (AM1.5d, 25 °C) [26]. The *IV*-characteristics under concentration were determined with a Flash simulator with four independently controlled light paths (concentration times AM1.5d spectrum at 1000 W/m^2 and 25 °C) [28]. All *IV*-curves were measured with a shadow mask to exactly define the designated cell area (~4.5 mm^2) and ensure that no carriers from outside that area are collected.

IV. Results and Discussion

In the following section, the performance of the four-junction device is presented, discussed and put in the context with the modelling study in section II.

The *EQE* measurement of the four-junction device is shown in Fig. 5. The bandgaps have been assessed from the *QE* using the methodology in Ref. [29], confirming that the implemented bandgaps are in good agreement with the nominal values (compare Fig. 1). Thus, the cell basically exhibits the optimal bandgaps for a four-junction device (Table I) - the only significant difference is the slightly higher bandgap of the $Ga_{0.78}In_{0.22}As$ cell, which was chosen on purpose to compensate for the parasitic absorption in the n-GaSb bond layer. An absorption simulation of the implemented layer stack is included in Fig. 5, which is based on the transfer matrix method and described in Ref. [4].

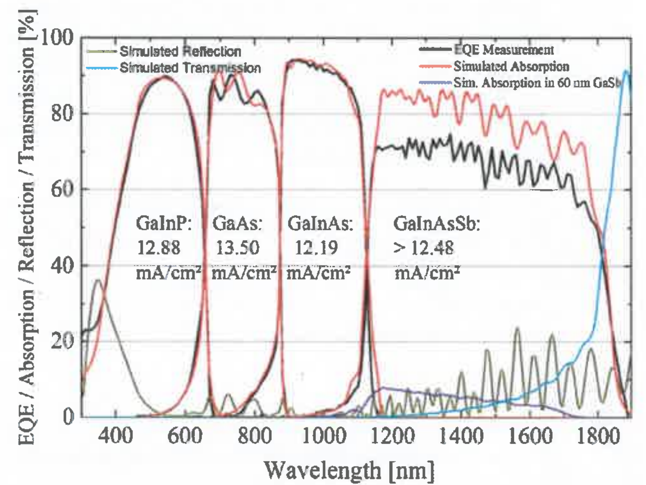

Fig. 5. Measured external quantum efficiency as well as simulated absorption, reflection and transmission of the Sb-based four-junction solar cell. The current densities of the subcells are calculated for the AM1.5d spectrum at 1000 W/m^2.

Considering the actual subcell thicknesses measured by scanning electron microscopy (SEM) as well as 5 % shading, the simulation agrees well with the measured *QE* - except for the absolute *QE* height of the bottom cell. Here, the measurement with a lock-in amplifier underestimates the *QE* due to a low parallel resistance of the bottom junction. The shunt could be identified in SEM measurements including energy-dispersive X-ray spectroscopy to result from Sb-oxides, which remained in the mesa trenches after the wet-chemical etching. Hence, the absorption simulation is a more realistic estimation of the real *QE* height in junction 4, taking into account the SEM-measured thickness of 2900 nm for the $Ga_{0.98}In_{0.02}As_{0.018}Sb_{0.982}$ absorber as well as the 60 nm GaSb bond layer, which remained after CMP. The simulated absorption correlates to a current density of 14.54 mA/cm^2. Otherwise, the shape of the *QE* in the bottom cell is not influenced by shunts and is in line with the simulation, indicating that the cell is not diffusion limited. It should be noted that the uncertainty in the *QE* height has a negligible

impact on the further evaluation of the cell's performance. Even the current density of 12.48 mA/cm^2, determined from the measured *QE*, does not limit the overall current density.

The absorption simulation and SEM investigation confirm that the first and third junction exhibit nominal thicknesses (compare section II), but reveal that the thickness of the semi-transparent GaAs cell amounts to 2010 nm instead of the intended 1770 nm, which was caused by an incorrect control of the GaAs growth rate. This results in a limiting current density of 12.19 mA/cm^2 for the $Ga_{0.78}In_{0.22}As$ cell and an excess current of the GaAs cell. The overall agreement between the absorption simulation and the *QE* measurement in the top three subcells indicates that basically all photons reaching the absorber layers are utilized. That result speaks for high material qualities with functional barriers and sufficient minority carrier diffusion lengths.

The *IV*-characterizations under concentration are shown in Fig. 6. The theoretical V_{OC} dependency on the concentration C (last summand of Eq. (1) with $n_{id} = 1$) is included in the graph, at which the factor "4" represents the number of junctions. The curve has a constant offset of 570 mV to the radiative limit for a four-junction solar cell at this specific bandgap combination, as discussed below.

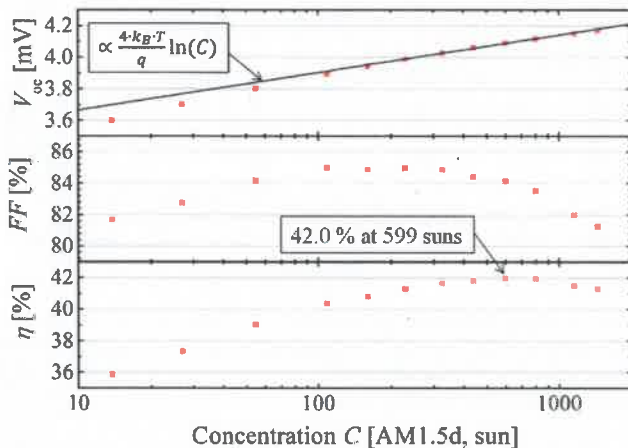

Fig. 6. Summary of the open-circuit voltage V_{OC}, fill factor *FF* and efficiency η of the Sb-based four-junction cell, determined by concentration-dependent *IV*-characterization.

The voltage increase at concentrations < 300 suns is higher than expected for ideal cells. As mentioned in section II, this increased voltage gain can be explained by the saturation of non-radiative defects, which is completed for concentrations > 300 suns. Then, the voltage follows the theoretical proportionality of Eq. (1) for ideal materials, which results for $C = 599$ in an averaged voltage gain of ~166 mV per junction. In addition to this expected gain, the total loss to the radiative limit is reduced from ~770 mV at 1 sun to ~570 mV at few hundred suns. That means that the saturation effects under concentration result in an additional 50 mV averaged voltage gain per junction.

The fill factor increases up to a concentration of 100 suns, which is mainly due to two effects. First, the impairment from the severe bottom cell shunt on the overall *FF* is decreasing for higher concentrations, due to saturation effects. Second, the influence of the rounded shape (exponential dependency) of an *IV*-curve on the *FF* decreases for higher voltages. These positive effects of the concentration on the *FF* are overcompensated at concentrations > 100 suns, at which the *FF* decreases due to the growing impact of the R_S.

In accordance with the evolution of V_{OC} and *FF*, the efficiency η increases significantly under concentration and reaches a maximum of 42.0 ± 2.5 % at a concentration of 599 suns.

The *IV*-curve at 599 suns is shown in Fig. 7, including a simulation of the measurement based on a 1-diode model. The simulation takes into account the measured bandgaps (Fig. 1), subcell currents (Fig. 5), cell area, concentration factor and a temperature of 298 K. A total voltage loss of 570 mV to the radiative limit, a total series resistance R_S of 23 mΩcm^2 and a total parallel resistance R_P of 350 Ω are used in the simulation to achieve an agreement between simulation and measurement. The only significant difference is in the rounding of the *IV*-curve at the maximum power point, which can be attributed to a distributed series resistance, which is a known effect for solar cells under concentration [30].

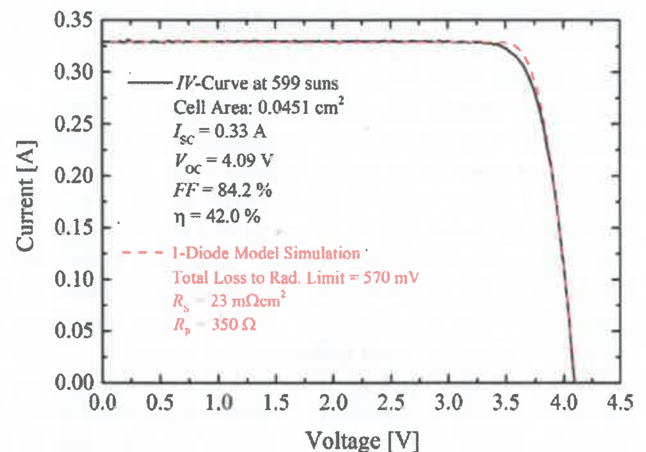

Fig. 7. *IV*-characteristic Sb-based four-junction solar cell at 599 suns, including a modelling based on a 1-diode model.

The 23 mΩcm^2 overall series resistance is mainly caused by the emitter sheet resistance in the $Ga_{0.51}In_{0.49}P$ cell as well as the front contact and the bond resistance, which both contribute a few mΩcm^2 to the R_S. The observable parallel resistance of ~350 Ω in Fig. 7 correlates to the R_P of the limiting $Ga_{0.78}In_{0.22}As$ subcell and is high enough to avoid any significant *FF* losses under concentration. The shunt in the bottom cell has a negligible impact on the *IV*-characteristic at 599 suns, as the shunt is mostly saturated. Still, junction 4 has a significantly lower *FF* than junction 3, but the excess current in the bottom cell is sufficient to exclude that its individual *IV*-curve does limit the overall current at any point.

The discussed solar cell results represent a promising starting point to further boost the efficiency of Sb-based four-junction solar cells in the short-term. The device has a high

current-mismatch of up to 2.35 mA/cm^2 (assuming the simulated 14.54 mA/cm^2 in the bottom cell). Current-matching is achievable by adapting the subcell thicknesses and choosing an optimal bandgap of 1.05 eV for the third subcell. Consequently, the overall current density may increase from 12.2 to ~13.3 mA/cm^2 and efficiencies > 44 % are reachable.

In the long-term, the cell has the potential to achieve > 50 % efficiency, as discussed in section II. The quantitative loss mechanisms of the implemented device in respect to this real-world efficiency target are estimated using the 1-diode model:

1. Current Losses: ~4.8 % absolute
2. Voltage Losses: ~1.5 % absolute
3. Fill Factor Losses: ~2.5 % absolute

In that context, it should be noted that these loss mechanisms also influence each other. The fill factor will drop when matching the subcell currents – otherwise, the potential efficiency gain from current would be even higher. In addition, the FF slightly increases for lower voltage losses – in this case the impact on the *IV*-curve rounding is decreasing.

Consequently, the experimental validation of the efficiency target requires several improvements to the four-junction solar cell. A further 0.9 mA/cm^2 can be gained by replacing the 60 nm GaSb bond layer by a non-absorbing layer and additional 0.7 mA/cm^2 by increasing the bottom cell thickness from 2900 to 4000 nm. Further current can be gained by minimizing the parasitic absorption in passive layers, like for example the tunnel-diodes. Finally, the material quality of all junctions has to be enhanced to achieve an average of 100 mV loss to the radiative limit per junction at concentrations of a few 100 suns and the series resistance has to be decreased to values below 15 $m\Omega cm^2$.

V. Conclusion

We have presented the modelling, fabrication and analysis of a wafer-bonded, two-terminal $Ga_{0.50}In_{0.50}P/GaAs/Ga_{0.78}In_{0.22}As//Ga_{0.98}In_{0.02}As_{0.018}Sb_{0.982}$ solar cell. This concept enables to realize the optimal bandgap combination for a monolithic four-junction device, which was modelled to be 1.89/1.42/1.05/0.68 eV. Even for five- and six-junction cells, the optimal bottom cell bandgap remains at ~0.68 eV if realistic voltage losses are taken into account.

The four-junction device is realized by separate epitaxial growth of an inverted top cell with three junctions and an upright bottom cell with one junction. The subcells are combined by argon-beam activated wafer bonding, enabling lowest bond resistances < 5 $m\Omega cm^2$ that do not significantly compromise the cell performance.

The semi-transparent GaAs subcell of the device was found to be 14 % too thick, taking some of the current away from the underlying $Ga_{0.78}In_{0.22}As$ subcell which in turn then limits the overall current density to 12.19 mA/cm^2. Under concentration, the increase in V_{OC} is higher than expected, which can be attributed to the saturation of non-radiative defects. The outcome is a 50 mV average voltage gain per junction at ~300 suns, in addition to the expected voltage gain for ideal cells. At concentrations > 300 suns, basically all defects are saturated, and the voltage increase is in line with the theoretical dependency. The efficiency peaks at 42.0 ± 2.5 % for a concentration of 599x AM1.5d.

The implemented cells represent a promising starting point to achieve an efficiency above 44% in the short-term, by matching the currents of all subcells. It has been shown that the concept has a realistic efficiency potential > 50 %. With respect to this efficiency target, further improvements can be made mainly in the device current (4.8 % abs. efficiency gain), but also in voltage (1.5 % abs. efficiency gain) and in fill factor (2.5 % abs. efficiency gain).

Acknowledgment

The authors would like to thank R. Freitas for the support in the processing of the solar cells and G. Siefer, M. Schachtner and E. Fehrenbach for assistance in the cell measurements. This work was funded by the German BMWi through the Project No. HekMod4 (Contract No. 0325750). F. Predan acknowledges the funding of his Ph.D. by the German Federal Environmental Foundation, DBU (Contract No. 20014/344).

References

[1] M. A. Green *et al.*, "Solar cell efficiency tables (version 50)," *Prog. Photovolt: Res. Appl.*, vol. 25, no. 7, pp. 668–676, 2017.

[2] W. Guter *et al.*, III-V Multijunction Solar Cells - New Lattice-Matched Products And Development Of Upright Metamorphic 3J Cells," in *7th International Conference on Concentrating Photovoltaic Systems (CPV-7): AIP Conference Proceedings 1407*, Las Vegas, Nevada, (USA), 2011.

[3] R. R. King *et al.*, "Solar cell generations over 40% efficiency," *Prog. Photovolt., Res. Appl.*, vol. 20, no. 6, pp. 801–815, 2012.

[4] F. Dimroth *et al.*, "Four-Junction Wafer-Bonded Concentrator Solar Cells," *IEEE J. Photovolt.*, vol. 6, no. 1, pp. 343–349, 2016.

[5] R. M. France *et al.*, "Design Flexibility of Ultrahigh Efficiency Four-Junction Inverted Metamorphic Solar Cells," *IEEE J. Photovolt.*, no. 6 (2), pp. 578–583, 2016.

[6] M. P. Lumb *et al.*, "GaSb-Based Solar Cells for Full Solar Spectrum Energy Harvesting," *Adv. Energy Mater.*, vol. 7, no. 20, p. 1700345, 2017.

[7] F. Predan *et al.*, "Developments for Wafer-bonded Four-Junction Solar Cells based on Gasb," in *2018 IEEE 7th World Conference on Photovoltaic Energy Conversion (WCPEC) (A Joint Conference of 45th IEEE PVSC, 28th PVSEC & 34th EU PVSEC)*, Waikoloa Village, HI, USA, 2018, pp. 1–6.

[8] D. R. Myers, K. Emery, and C. Gueymard, "Proposed reference spectral irradiance standards to improve concentrating photovoltaic system design and performance evaluation," in *Conference Record of the*

29th IEEE Photovoltaic Specialists Conference: Hyatt Regency New Orleans, New Orleans, Louisiana, May 19-24, 2002, New Orleans, Louisiana, USA, 2002, pp. 923–926.

[9] G. Létay and A. W. Bett, "EtaOpt - a program for calculating limiting efficiency and optimum bandgap structure for multi-bandgap solar cells and TPV cells," in *Proceedings of the 17th European Photovoltaic Solar Energy Conference and Exhibition*, Munich, Germany, 2001, pp. 178–181.

[10] S. P. Philipps and A. W. Bett, "III-V Multi-junction solar cells and concentrating photovoltaic (CPV) systems," in *Advanced Optical Technologies*, pp. 469–478.

[11] W. Shockley and H. J. Queisser, "Detailed balance limit of efficiency of *p-n* junction solar cells," *J. Appl. Phys.*, vol. 32, no. 3, pp. 510–519, 1961.

[12] O. D. Miller, E. Yablonovitch, and S. R. Kurtz, "Strong internal and external luminescence as solar cells approach the shockley-queisser limit," *IEEE J. Photovolt.*, vol. 2, no. 3, pp. 303–311, 2012.

[13] J. F. Geisz *et al.*, "Implications of Redesigned, High-Radiative-Efficiency GaInP Junctions on III-V Multijunction Concentrator Solar Cells," *IEEE J. Photovolt.*, vol. 5, no. 1, pp. 418–424, 2015.

[14] J. F. Geisz *et al.*, "Enhanced external radiative efficiency for 20.8% efficient single-junction GaInP solar cells," (English), *Appl. Phys. Lett.*, vol. 103, no. 4, 041118 (5 pp.), 2013.

[15] C. L. Schilling *et al.*, "Combining Photon Recycling and Concentrated Illumination in a GaAs Heterojunction Solar Cell," *IEEE J. Photovolt.*, vol. 8, no. 1, pp. 348–354, 2018.

[16] B. M. Kayes *et al.*, "27.6% conversion efficiency, a new record for single-junction solar cells under 1 sun illumination," in *Conference Record of the 37th IEEE Photovoltaic Specialists Conference*, Seattle, WA, USA, 2011, pp. 4–8.

[17] J. F. Geisz *et al.*, "Building a Six-Junction Inverted Metamorphic Concentrator Solar Cell," *IEEE J. Photovoltaics*, vol. 8, no. 2, pp. 626–632, 2018.

[18] H. K. Choi *et al.*, "High-performance GaInAsSb thermophotovoltaic devices with an AlGaAsSb window," (English), *Appl. Phys. Lett.*, vol. 71, no. 26, pp. 3758–3760, 1997.

[19] C. A. Wang *et al.*, "Recent progress in GaInAsSb thermophotovoltaics grown by organometallic vapor-phase epitaxy," *J. Cryst. Growth*, vol. 195, no. 1-4, pp. 346–355, 1998.

[20] F. Predan *et al.*, "Hall characterization of epitaxial GaSb and AlGaAsSb layers using p-n junctions on GaSb substrates," *J. Cryst. Growth*, vol. 496-497, pp. 36–42, 2018.

[21] F. Predan *et al.*, "Developments for Wafer-bonded Four-Junction Solar Cells based on Gasb," in *Proceedings of the 7th World Conference on Photovoltaic Energy Conversion*, Waikoloa, Hawaii, 2018, pp. 1–6.

[22] F. Predan *et al.*, "Transparent and electrically conductive GaSb/Si direct wafer bondingat low temperatures by argon-beam surface activation," *Appl. Surf. Sci.*, vol. 353, pp. 1203–1207, 2015.

[23] F. Predan *et al.*, "Effects of thermal annealing on structural and electrical properties of surface-activated n-GaSb/n-GaInP direct wafer bonds," *Journal of Applied Physics*, vol. 122, no. 13, p. 135307, 2017.

[24] F. Predan *et al.*, "Direct wafer bonding of highly conductive GaSb/GaInAs and GaSb/GaInP heterojunctions prepared by argon-beam surface activation," *J. Vac. Sci. Technol. A-Vac. Surf. Films*, vol. 34, no. 3, p. 31103, 2016.

[25] M. M. R. Howlader, A. Yamaguchi, and T. Suga, "Surface activation-based nanobonding and interconnection at room temperature," *J. Micromech. Microeng.*, vol. 21, no. 2, 025009 (10 pp.), 2011.

[26] M. Meusel *et al.*, "Spectral Mismatch Correction and Spectrometric Characterization of Monolithic III-V Multi-junction Solar Cells," *Prog. Photovolt., Res. Appl.*, vol. 10, no. 4, pp. 243–255, 2002.

[27] G. Siefer, C. Baur, and A. W. Bett, "External quantum efficiency measurements of Germanium bottom subcells: Measurement artifacts and correction procedures," in *Conference Record of the 35th IEEE Photovoltaic Specialists Conference*, Honolulu, HI, USA, 2010, pp. 704–707.

[28] M. Schachtner *et al.*, "Analysis of a four lamp flash system for calibrating multi-junction solar cells under concentrated light," in *11th International Conference on Concentrator Photovoltaic Systems (CPV-11): AIP Conference Proceedings 1679*, Aix-les-Bains, France, 2015, p. 50012.

[29] H. Helmers, C. Karcher, and A. W. Bett, "Bandgap determination based on electrical quantum efficiency," *Appl. Phys. Lett.*, vol. 103, no. 3, 032108 (3pp.), 2013.

[30] M. Steiner *et al.*, "Validated front contact grid simulation for GaAs solar cells under concentrated sunlight," *Prog. Photovolt., Res. Appl.*, vol. 19, no. 1, pp. 73–83, 2010.